I&EC research
Industrial & Engineering Chemistry Research

Article

pubs.acs.org/IECR

Effects of Finite Size and Proton Disorder on Lattice-Dynamics Estimates of the Free Energy of Clathrate Hydrates

Sabry G. Moustafa, Andrew J. Schultz, and David A. Kofke*

Department of Chemical and Biological Engineering, University at Buffalo, The State University of New York, Buffalo, New York 14260-4200, United States

Supporting Information

ABSTRACT: We consider lattice dynamics methods for calculation of the free energy of clathrate hydrate phases, specifically the cubic structure I (sI), cubic structure II (sII), and hexagonal structure H (sH) phases, in the absence of guest molecules; water molecules are modeled with the TIP4P potential. We examine in particular the effects of finite size and proton disorder on the calculated free energies and consider these in the context of the free-energy differences between the phases. We find that at 300 K, the finite-size, proton-disorder, and quantum effects between phases are, respectively, on the order of 0.4, 0.03, and 0.1 kJ/mol. Details of the calculations are provided, with emphasis on efficiencies developed to handle various aspects related to rigid-molecule lattice dynamics with electrostatic interactions in large crystalline systems.

1. INTRODUCTION

Clathrate hydrates are crystalline compounds formed from water and small hydrophobic solutes (e.g., methane) in which the water molecules form a lattice of hydrogen-bonded polyhedral cages, each surrounding one or perhaps a few of the solute (guest) molecules.[1,2] Clathrates are important for both technological and environmental reasons. From a technological standpoint, the formation of clathrates is a major concern in the oil and gas industry, where undesired formation in pipelines produces solid plugs that halt flow. Consequently, significant effort is directed toward flow assurance by prevention or control of the formation of clathrate hydrates. A more positive technological issue is in the exploration of clathrates as a means for storage and transport of gaseous fuels, particularly methane and even hydrogen,[3−5] or for sequestration of pollutants and greenhouse gases, especially carbon dioxide.[6] Natural stores of methane in permafrost or seafloor hydrates are huge,[7] and recovery of this resource, particularly in conjunction with a complementary process to sequester CO_2, could provide a long-term energy source to meet worldwide demand. Other uses envisioned for clathrate hydrates include gas separation,[8] desalination,[9] and refrigeration.[10,11]

Clathrate compounds are nonstoichiometric, in that some of the cages may be vacant or have multiple occupancy at equilibrium. The lattice of empty cages is mechanically stable, but there is a minimum occupancy required for thermodynamic stability. Hydrates appear in several structures, each of which combines two or more cage types to form a unit cell, and differing in the size, shape, and number of cages in the repeat unit. The most common structures[2,12] are structure I (sI, with 2 small + 6 large cages formed from 46 water molecules in the unit cell),[13] structure II (sII, 16 + 8 cages from 136 water molecules),[14] and (less common) structure H (sH, 3 + 2+1 cages from 34 waters).[15] The structure adopted by a clathrate hydrate generally depends on the size of the solute molecule.

Given their practical importance, it is not surprising that these compounds have received an intense amount of attention from the research community. They have been studied by experiment for centuries.[1] It has been found that thermodynamic behavior is for many purposes adequately described by the van der Waals−Platteeuw (vdWP) model.[16,17] This is a statistical-mechanical theory that treats the hydrate as individual cages housing guest molecules that do not interact across cages. It further assumes single occupancy of the cages, that occupancy of one cage has no effect on others, and that quantum effects can be neglected. Various extensions have relaxed one or more of these assumptions. However, selective removal of approximations might in fact be counterproductive, as molecular simulation studies[18−20] have found that the vdWP model gains some accuracy through a cancellation of errors. The ability of molecularly detailed modeling to provide insights such as this, coupled with many advances in methods, models, and computing hardware in recent years, has led to increasing interest in these approaches as a route to understand, predict, and manipulate clathrate behavior.

Of central importance to all modeling studies is knowledge of the thermodynamic phase behavior of the system being modeled. Often this information is useful as an end in itself, for example when the study aims to gauge the number of guest molecules that can occupy the cages of a given clathrate structure under different conditions.[21−26] Knowledge of the phase behavior is important also as a backdrop for other studies, such as those relating to nucleation and growth.[27] Interpretation of molecular simulation data for these processes cannot be made conclusive without knowledge of the stability boundary and thermodynamic forces driving the behavior.[12,32]

Special Issue: Scott Fogler Festschrift

Received: October 10, 2014
Revised: November 26, 2014
Accepted: December 1, 2014
Published: December 1, 2014

   dx.doi.org/10.1021/ie504008h | Ind. Eng. Chem. Res. 2015, 54, 4487−4496

Inasmuch as thermodynamic properties for different molecular models do not in general coincide with each other (or with experimental behavior), it is necessary to gather these data for the specific molecular model underlying the (for example) nucleation studies.

Free-energy calculations in molecular simulation are often problematic or computationally expensive, although they are becoming routine. Still, applications to clathrate hydrate structures introduce special difficulties, and relatively few rigorous absolute free-energy calculations have been conducted for these systems[18,28−31,33,34] (we exclude here free-energy calculations and grand-canonical simulations that yield cage-occupancy statistics, given the clathrate structure). Much more common are studies employing harmonic[35,36] and quasi-harmonic[22−24,37−39] treatments based in lattice dynamics. These approaches are approximate and are limited to the range of (low) temperatures where the harmonic approximation is correct. Nevertheless, they represent an important component in the collection of methods available for the modeling of clathrate systems, and indeed crystalline water (ice)[40−43] phases in general: they are much faster than molecular simulation in yielding values of thermodynamic properties; they have no difficulty capturing the quantum nature of oscillation that prevails at low temperatures; they provide a suitable starting point for more rigorous molecular simulation studies.[44] In particular, thermodynamic integration from a low-temperature state, where the harmonic treatment is accurate, provides a convenient route to the free energy at an arbitrary condition of interest. Moreover, it has been observed[45−48] that finite-size effects inherent in molecular simulations of solids are largely due to the harmonic behavior of the crystal. This means that molecular simulation methods that isolate anharmonic effects can be applied to measure properties for relatively small systems without incurring finite-size errors, and the infinite-system harmonic behavior can be added afterward to yield the full behavior in the thermodynamic limit.

The assumption that the energy can be modeled using a harmonic expansion about a minimum-energy configuration is not the only approximation inherent in practical lattice-dynamics calculations of hydrates and ice phases. Given the foundational role held by lattice dynamics methods for the study of these systems, it is worthwhile to examine some of these other approximations. First, it is well-known that crystalline structures of water are often proton-disordered, meaning that the orientations of the water molecules are not uniquely specified as part of the crystal structure.[49] Within certain constraints, there are many possible structural isomers, each differing in the way that the water molecules are each oriented. The usual practice is to select a low-energy isomer with near-zero dipole moment and perform lattice dynamics calculations using this single structure. Sometimes multiple structures are used, and properties are averaged in a simple manner. In the present work, we examine the suitability of such approaches. Second, we consider finite-size effects and how the free energy extrapolates to the thermodynamic limit. Such understanding is needed if we aim to use the harmonic system as a reference that captures the large-system behavior when coupled to (small-system) molecular simulations that correct for anharmonic effects. Finally, some studies[50−52] make use of a more approximate local-harmonic approach, which is a mean-field treatment in which each molecule oscillates in a field imposed by the others, effectively forming an Einstein crystal with anisotropic force constants determined by interactions with the other molecules. The suitability of this approximation is easily tested as part of the overall study.

This paper is organized as follows. In the following section we describe the models and methods used for the harmonic free-energy calculations. In section 3, we present the results of the calculations, and in section 4 we provide a summary and conclusions. We also include additional details about the lattice dynamics calculations in the Supporting Information.

2. THEORY AND METHODS

2.1. Harmonic Analysis of Rigid Molecules. In this section, we review the framework for estimating the free energy, under the assumption that the intermolecular interactions can be approximated by a harmonic potential. We develop the methods for application to a single proton-disordered structure, which we take as given. Approaches for accounting for proton disordering will be described in section 2.2.

The normal modes of motion of flexible molecules are classified into "external" (translation and rotation of the whole molecule) and "internal" (internal vibrations and bending). In this work, we use a rigid model for the water molecule, for which only external modes are present. Accordingly, we focus our review on the harmonic analysis of the external modes of nonlinear rigid molecules. The concepts and methods are all well established,[53−56] so we will not attempt to be complete. Instead we will highlight the key steps in the treatment needed to understand the contributions made in this work, while pointing out some novel features in our implementation.

For nonlinear rigid molecules, in addition to the three translational degrees of freedom (dof), three angular dof per molecule are required to fully describe the system configuration. The linear and angular displacements of a molecule κ in cell l along the α direction will be denoted by $u^t_\alpha(l\kappa)$ and $u^r_\alpha(l\kappa)$, respectively. $u^t_\alpha(l\kappa)$ represents the translational deviation of molecule κ's center of mass (CM) from its equilibrium position. Concerning rotation, there are several choices for an appropriate definition of $u^r_\alpha(l\kappa)$; the only requirement is to be able to use them to expand the potential energy. The most common choice is the angle of rotation around α axis (adopting the right-hand rule) with respect to its nominal orientation in the crystal. For small rotations, the rotation can be decomposed into three rotations around x, y, and z axes (θ_x, θ_y, and θ_z), respectively.

In the sums that follow, κ goes over all n molecules in unit cell l; α and β go over all coordinate directions, x, y, z; i goes over t and r for translation and rotation; and l goes over N_c replicas of the unit cell (all having the same proton-disordered structure), forming a supercell. The number of molecules in the supercell, N, equals nN_c. Primes on each of these indices are used to form a second set of sums.

The potential energy U includes interactions among all of the N molecules of the supercell and may (as it does here) include interactions of these N molecules with an (in principle) infinite periodic system surrounding it (evaluated in practice via a combination of lattice and Ewald sums). One of our interests in this work is how the free energy approaches the thermodynamic limit with increasing N when U is estimated via a harmonic potential. Accordingly, U is approximated via a Taylor expansion in molecular displacements (both linear and angular) as follows:[55]

dx.doi.org/10.1021/ie504008h | Ind. Eng. Chem. Res. 2015, 54, 4487−4496

$$U \approx U_0 + \frac{1}{2}\sum_{\substack{lk\alpha\\ l'k'\beta}}\left(\frac{\partial^2 U}{\partial u_\alpha^t(lk)\,\partial u_\beta^t(l'k')}\right)_0 u_\alpha^t(lk)\,u_\beta^t(l'k') + \frac{1}{2}\sum_{\substack{lk\alpha\\ l'k'\beta}}\left(\frac{\partial^2 U}{\partial u_\alpha^r(lk)\,\partial u_\beta^r(l'k')}\right)_0 u_\alpha^r(lk)\,u_\beta^r(l'k') + \frac{1}{2}\sum_{\substack{lk\alpha\\ l'k'\beta}}\left(\frac{\partial^2 U}{\partial u_\alpha^t(lk)\,\partial u_\beta^r(l'k')}\right)_0 u_\alpha^t(lk)\,u_\beta^r(l'k') + \frac{1}{2}\sum_{\substack{lk\alpha\\ l'k'\beta}}\left(\frac{\partial^2 U}{\partial u_\alpha^r(lk)\,\partial u_\beta^t(l'k')}\right)_0 u_\alpha^r(lk)\,u_\beta^t(l'k') \quad (1)$$

which is truncated at second order. We omit the terms linear in $u_\alpha^i(lk)$ because the derivatives are evaluated with all molecules at their respective equilibrium (minimum energy, U_0) positions and orientations, and consequently all first derivatives with respect to both linear and angular displacements (i.e., forces and torques) vanish. We are left here with only the second-order contribution, representing the harmonic approximation to the energy, U_{harm} (defined in excess of U_0). The harmonic energy can be written more compactly in terms of generalized force-constant coefficients, $\varphi_{\alpha\beta}^{ii'}(lk;l'k')$, defined by

$$\varphi_{\alpha\beta}^{ii'}(lk;\,l'k') = \left(\frac{\partial^2 U}{\partial u_\alpha^i(lk)\,\partial u_\beta^{i'}(l'k')}\right)_0 \quad (2)$$

as follows

$$U_{\mathrm{harm}} = \frac{1}{2}\sum_{\substack{ll',kk'\\ \alpha\beta,ii'}}\varphi_{\alpha\beta}^{ii'}(lk;\,l'k')\,u_\alpha^i(lk)\,u_\beta^{i'}(l'k') \quad (3)$$

With the energy approximated as in eq 3, we are left with a system of coupled harmonic oscillators, for which the dynamics and thermodynamics can be evaluated analytically. The conventional approach is to solve for the dynamical behavior, which yields a set of frequencies ω_j for what are effectively a set of independent harmonic oscillators, each describing some collective motion of the molecules. The partition function of a harmonic oscillator can be easily evaluated for both the quantum and classical cases,[57] and from these expressions the free energy can be written as a sum of contributions over all frequencies. Thus, classically,

$$\beta A_{\mathrm{harm}} = \sum_j \ln\left(\frac{\hbar\omega_j}{k_{\mathrm{B}}T}\right) + \beta A^{\mathrm{CM}} + N\ln s_{\mathrm{rot}} \quad (4)$$

and for the quantum oscillator,

$$\beta A_{\mathrm{harm}} = \sum_j \ln\left[2\sinh\left(\frac{\hbar\omega_j}{2k_{\mathrm{B}}T}\right)\right] + \beta A^{\mathrm{CM}} + N\ln s_{\mathrm{rot}} \quad (5)$$

where k_{B} is Boltzmann's constant, T is the temperature, $\beta = 1/k_{\mathrm{B}}T$, $\hbar = h/2\pi$ with h Planck's constant, s_{rot} is the number of proper rotations of the molecule (2 for H_2O), and A^{CM} is the center-of-mass correction to the free energy, which is given by[45]

$$\beta A^{\mathrm{CM}} = -\frac{d}{2}\ln N + \ln\rho \quad (6)$$

in which $d = 3$ is the number of spatial dimensions, and ρ is the molecule number density. The number of frequencies in the sum is $6N - 3$, which is the total dof of the system, minus those corresponding to translation of the whole supercell in the three coordinate directions.

We now review the procedure for evaluation of the frequencies ω_j. The process begins with the equations of motion for the displacements $u_\alpha^i(lk)$, expressing the change in linear and angular momenta in terms of the forces and torques that correspond to eq 3. The lattice symmetry dictates a plane-wave solution, which when substituted into the equations of motion yields a determinantal equation for the frequencies:[55,56]

$$|\mathbf{D}(\mathbf{k}) - \omega^2(\mathbf{k})\mathbf{M}| = 0 \quad (7)$$

where $\mathbf{D}(\mathbf{k})$ is the $6n \times 6n$ dynamical matrix with elements

$$D_{\alpha\beta}^{ii'}(\mathbf{k},\,\kappa\kappa') = \sum_{l'}\varphi_{\alpha\beta}^{ii'}(0\kappa;\,l'\kappa')\exp[i\mathbf{k}\cdot\mathbf{l}'] \quad (8)$$

(note that i in the exponential here is $(-1)^{1/2}$). The $6n \times 6n$ matrix $\mathbf{M}$ in eq 7 has the molecule masses and 3×3 inertia tensors on its diagonal.[55,56] The vector $\mathbf{l}'$ is the Cartesian position (with respect to an origin at $l = 0$) of the lattice site indexed by l'. It is interesting to mention here that one can reach the same classical free energy result using a different route that avoids computing $\mathbf{M}$ while diagonalizing the force constant matrix directly. Elsewhere,[58] we demonstrate mathematically and numerically the equivalence between the two approaches. However, this alternative approach cannot be used in the quantum treatment; *i.e.* one must always solve eq 7.

The wave vectors $\mathbf{k}$ are those allowed from the first Brillouin zone of the supercell. That is, if we have a supercell formed from $n_{c1} \times n_{c2} \times n_{c3}$ unit cells in the respective lattice-vector directions (a_1,a_2,a_3), then the allowable values of $\mathbf{k}$ are $\mathbf{k} = (m_1/n_{c1})\mathbf{b}_1 + (m_2/n_{c2})\mathbf{b}_2 + (m_3/n_{c3})\mathbf{b}_3$, where $(\mathbf{b}_1, \mathbf{b}_2, \mathbf{b}_3)$ are the reciprocal-lattice vectors of the unit cell, and where m_i are integers satisfying $-n_{ci} < 2m_i \le n_{ci}$. Thus, for the $1 \times 1 \times 1$ supercell we have only $\mathbf{k} = 0$; for $2 \times 2 \times 2$ we have eight values of $\mathbf{k}$ formed from each of the $m_i = \{0,1\}$; for $3 \times 3 \times 3$ we have 27 values, $m_i = \{-1,0,1\}$; for $4 \times 4 \times 4$ we have 64 values, $m_i = \{-1, 0, 1, 2\}$; *etc.*

For each $\mathbf{k}$, the solution of eq 7 yields $6n$ values of the frequency ω_i. We need not perform the eigenvalue calculation for all allowable wave vectors, because we can exploit the Hermiticity of the dynamical matrix, from which we know that $\omega(-\mathbf{k}) = \omega(\mathbf{k})$.[59] It should also be noted that the calculation of the derivatives $\varphi_{\alpha\beta}^{ii'}(0\kappa;\ l'\kappa')$—each of which involves convergence of a lattice sum of Lennard-Jones interactions and an Ewald sum—need be performed just once for each $(\alpha\beta\kappa\kappa' ii' l')$, and in particular they do not have to be recomputed for each of the wave vectors. This economy provides a significant computational advantage over an approach that includes the wave vector $\mathbf{k}$ in the lattice and Ewald sums for φ.[56]

Additional detail regarding the lattice dynamics calculations may be found in the Supporting Information.

2.2. Proton Disorder. As mentioned above, the crystal structure of a clathrate hydrate specifies the positions of only the oxygen atoms. The hydrogen (proton) positions are not specified, but their arrangement nominally must satisfy the Bernal−Fowler ice rules.[60,61] These rules state that each oxygen is covalently bonded to two hydrogens, each oxygen forms two hydrogen bonds to two other oxygens, and there exists exactly

dx.doi.org/10.1021/ie504008h | Ind. Eng. Chem. Res. 2015, 54, 4487−4496

Table 1. TIP4P Potential Model Parameters[65]

r_{OH} (Å)	∠HOH (deg)	r_{OM} (Å)	A (kcal Å^{12}/mol)	C (Å^6/mol)	q_O (e)	q_H (e)	q_M (e)
0.9572	104.52	0.15	600.0×10^3	610.0	0.0	0.52	−1.04

Table 2. Real and Reciprocal Cutoff Parameters of Ewald Summation That Give Truncation Error in the Lattice Energy Less than 10^{-6} kJ/mol[a]

sI								
n_c	1	2	3	4	5	6	7	8
r_{cut} (Å)	14.00	19.34	23.36	26.69	29.60	32.21	34.59	36.79
k_{cut} (Å^{-1})	2.60	1.80	1.45	1.24	1.10	1.00	0.92	0.85
sII								
n_c	1	2	3	4	5			
r_{cut} (Å)	10.00	13.80	16.68	19.10	21.13			
k_{cut} (Å^{-1})	3.60	2.50	2.00	1.72	1.52			
sH								
n_c	1	2	3	4	5	6	7	
r_{cut} (Å)	20.00	27.69	33.48	38.30	42.50	46.28	49.72	
k_{cut} (Å^{-1})	2.00	1.38	1.12	0.96	0.85	0.77	0.71	

[a] n_c is the number of unit cells in each direction forming the supercell, such that $N_c = n_c^3$.

one hydrogen between a pair of neighboring oxygens (violations of these rules are known as Bjerrum defects[62]). In addition, it is usually taken that the water molecules must orient such that the structure as a whole has negligible dipole moment, because the bulk crystal has no dipole.

Absent any defects, the proton-disordered isomers may be treated as independent components of the overall partition function, such that the total free energy can be given as a sum over all isomers.[61] If we use ν to index the isomers, so that the free energy of the system constrained to isomer ν is $A(\nu)$, then the full free energy of the system is given by the sum over isomers:

$$\begin{aligned}\beta A &= -\ln \sum_{\nu} \exp[-\beta A(\nu)] \\ &\approx -\ln \sum_{\nu} \exp[-\beta(U_0(\nu) + A_{harm}(\nu))]\end{aligned} \tag{9}$$

where we separate A into its contributions from the static lattice energy and the harmonic vibrations, to emphasize that each depends on the isomer ν. Topologically identical proton arrangements are each represented in the sum; an alternative is to sum over distinct isomers and multiply by a degeneracy factor.

It is not a trivial task to evaluate the number of isomers that comply with the ice rules, but Pauling estimated[63] the number of isomers as $(3/2)^N$, and this has been shown to be accurate enough for many purposes. Thus, the sH structure, which with 34 water molecules has the smallest unit cell, has about 1 million isomers for the single unit cell. Many of these will have a non-negligible dipole moment, and would be excluded on that basis, but this would not be known until they were generated and examined. With such a number, consideration of all possible isomers is not feasible; so instead we can sample them, using M samples. Accordingly, we estimate the proton-disordered free energy as

$$\begin{aligned}\beta A &= -\ln\left(\frac{1}{M}\sum_{\nu}^{M} \exp[-\beta A(\nu)]\right) - N \ln(3/2) \\ &= \beta\langle U_0 + A_{harm}\rangle_{exp} - N \ln(3/2)\end{aligned} \tag{10}$$

which uses Pauling's value for the total number of terms in the sum represented by the sample; we use $\langle ... \rangle_{exp}$ to represent the exponential average. In many cases, a single sample ν_i is used, typically the one having the lowest energy and a negligible dipole. Effectively, the assumption is that the free energy is the same for all terms in the sum over ν, and eq 9 becomes

$$\beta A = \beta[U_0(\nu_i) + A_{harm}(\nu_i)] - N \ln(3/2) \tag{11}$$

It has been observed[61] that A_{harm} varies less than U_0 does across different isomers, leading to an approximation in which U_0 is averaged while a single representative value is used for A_{harm}:

$$\begin{aligned}\beta A &= -\ln\left(\frac{1}{M}\sum_{\nu}^{M} \exp[-\beta U_0(\nu)]\right) + \beta A_{harm}(\nu_i) \\ -N \ln(3/2) &= \beta\langle U_0\rangle_{exp} + \beta A_{harm}(\nu_i) - N \ln(3/2)\end{aligned} \tag{12}$$

One also sees this approach employed but using instead a simple arithmetic average of U_0:[41]

$$\begin{aligned}\beta A &= \frac{1}{M}\sum_{\nu}^{M} \beta U_0(\nu) + \beta A_{harm}(\nu_i) - N \ln(3/2) \\ &= \beta\langle U_0\rangle + \beta A_{harm}(\nu_i) - N \ln(3/2)\end{aligned} \tag{13}$$

2.3. Computational Details. Three different empty crystalline structures were considered, viz., sI, sII, and sH. sI is a cubic system with the *Pm*3*n* space group and contains 46 H_2O molecules per unit cell; sII is a face-centered cubic system with the *Fd*3*m* space group and contains 136 H_2O molecules per unit cell; and sH is a hexagonal system with the *P*6/*mmm* space group and contains 34 H_2O molecules per unit cell. The lattice parameters of the sI and sII cubic systems used here are 12.03 Å, and 17.31 Å, respectively.[1,49] We combine two sH hexagonal unit cells to form an orthorhombic 68-molecule unit cell with dimensions 12.21 Å × 21.15 Å × 10.14 Å.[1,49] The coordinates of the oxygen atoms in the hydrate structures are determined by X-ray diffraction;[13] in this work we used the oxygen positions given in ref 49 as initial (unminimized) coordinates. The positions of protons (hydrogen atoms) are

dx.doi.org/10.1021/ie504008h | Ind. Eng. Chem. Res. 2015, 54, 4487−4496

generated using the algorithm described by Buch et al.,[64] which satisfies the ice rules.[60]

The TIP4P force-field model[65] was employed for the intermolecular interactions between the H_2O molecules. TIP4P is a rigid four-site model: three charged sites (on H_1, H_2, and M) and one 12−6 Lennard-Jones (LJ) site (on O). Table 1 shows the TIP4P parameters.

Lattice sums were evaluated for the LJ interactions between the oxygen atoms. The LJ cutoff (R_{cut}) is set equal to 400 Å for both sI and sII and 500 Å for sH, to make sure that the truncation error in the energy is less than 10^{-6} kJ/mol. We employed a plain Ewald summation (ES) technique[66] for the long-range Coulomb interactions. We set the ES real (r_{cut}) and reciprocal (k_{cut}) cutoffs such that the truncation errors in the real and reciprocal energies are on the same order of magnitude and less than 10^{-6} kJ/mol based on the Kolafa and Perram[67] formula for the truncation errors. Table 2 shows the specific cutoffs for different structures and supercell sizes used in this study.

The force-constant matrix for the local-harmonic approximation[68] is exactly the same as that for the full harmonic analysis, except that only the 3 × 3 block matrices (self-linear and angular interactions) along the diagonal of the full matrix are kept, while other interaction energies are set to zero. Hence there is no need to compute any other terms to implement this approximation.

3. RESULTS AND DISCUSSION

3.1. Structures Generation and Relaxation. Using Buch et al.'s algorithm,[64] 5000 proton-disordered structures were generated for each hydrate structure. Figure 1 shows the

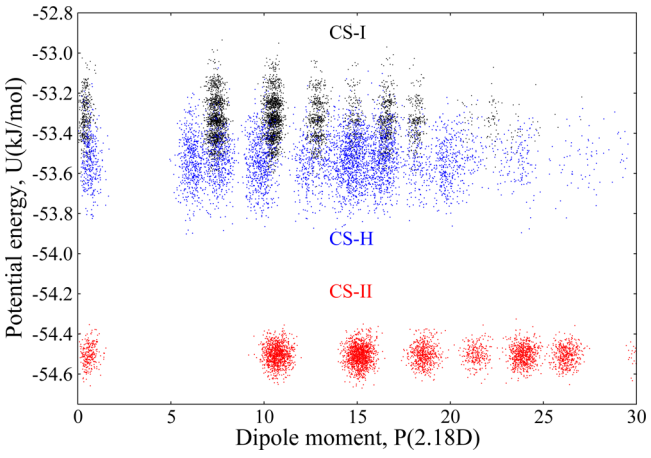

Figure 1. Potential energy versus the net dipole moment of the proton-disordered sI, sII, and sH hydrate structures generated in this study.

relationship between the potential energy and the net dipole moment of those structures. The average values of the potential energy are −53.3301, −54.5052, and −53.5343 kJ/mol for sI, sII, and sH, respectively. The dipole moments fall into bands that are in agreement with those computed by Takeuchi.[49] For each structure, 100 of the 5000 H-isomers with the smallest dipole moment (regardless of energy) were chosen to compute the free energy.

For the purpose of harmonic analysis, all molecules must be at their respective minimum-energy positions and orientations. We employed the steepest descent method to relax the molecular coordinates for the 100 H-isomer structures of each hydrate. Several minimization steps (∼200) were performed until the forces and torques on all molecules were on the order of 10^{-4} (in units of Å, Dalton, and ps). Among the 100 H-isomers, the structure with the minimum lattice energy was selected for computing the free energy as will be shown below. Those structures have potential energies before (after) minimization of −54.068731 (−55.263099), −54.768947 (−55.400356), and −54.175096 (−55.262875) kJ/mol.

3.2. H-Isomer Averaging. Since both the lattice and the harmonic free energies enter into the exponential averaging formula, eq 9, the variation in both quantities affect the final free-energy results. We found that the standard deviations of U_0 are ∼0.03, 0.01, 0.02 kJ/mol, and those of A_{harm} are ∼2.31 × 10^{-5} T, 7.06 × 10^{-6} T, and 2.86 × 10^{-5} T kJ/mol (where T is in K) for sI, sII, and sH, respectively: the variation in U_0 dominates over that of A_{harm}, and hence, it is reasonable to consider only one isomer for the harmonic free energy and average over the potential energy (*i.e.*, the approximation given by eq 12). Figure 2 shows the free-energy error (relative to the

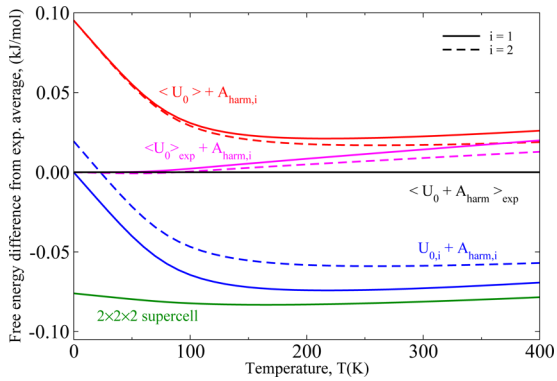

Figure 2. The 1 × 1 × 1 sI harmonic free energy using various approximations (viz. eq 11 (blue), eq 12 (magenta), and eq 13 (red)) expressed as a difference from the full exponential average (eq 10). Approximations using two isomer choices are shown: the i = 1 H-isomer (solid lines) is the structure with the minimum lattice energy, and i = 2 is the second-lowest one (dashed lines). The green line (labeled 2 × 2 × 2) is the same as the blue solid line but using a 2 × 2 × 2 supercell and with the single isomer being a replica of the i = 1 unit cell.

full exponential average of 100 isomers, eq 10) resulting from different approximations using the lowest-energy (solid line, i = 1) or second-lowest-energy (dashed line, i = 2) H-isomers of 1 × 1 × 1 sI hydrates. For the temperature range studied here (0 to 400 K), considering i = 1, exponential averaging of U_0 with a single-isomer A_{harm} (magenta curve, eq 12) produced the smallest error (<0.025 kJ/mol), while using a single isomer for U_0 (blue curve, eq 11) incurs larger error (∼0.07 kJ/mol for T > 100 K). The approximation based on the arithmetic average of the lattice energy, denoted by ⟨...⟩, (red curve, eq 13),[41] produces large error at lower temperatures and approaches (as expected) the full exponential average at higher temperatures. Comparison of the curves for the two isomers indicates that, given that the selected isomer is among those having the lowest energy, the free energy is less sensitive to the choice of isomer than to the choice of approximation.

3.3. Finite-Size Effects: Thermodynamic Limit. We perform extrapolation to the thermodynamic limit by computing free energies for supercells of increasing size N

dx.doi.org/10.1021/ie504008h | Ind. Eng. Chem. Res. 2015, 54, 4487−4496

and examining the limit as $1/N \rightarrow 0$. The supercell sizes used for each clathrate structure are given in Table 2. In principle, the free energy computed for each supercell size should employ averaging over isomers, as described in the previous section. Moreover, rather than use a supercell formed from replicas of a common proton-disordered unit cell, we should use a "unit-supercell" in which proton disordering is performed across the entire structure. We will use "exponential-average correction" (EAC) to refer to the difference between the free energy for the proper isomer-averaged treatment, and that for the single (nonaveraged) replicated-isomer supercell used for the extrapolation. The computational expense involved in computing the EAC grows considerably with N, which has led us to instead use an approximation. Specifically, we estimate the free energy in the thermodynamic limit by extrapolating the free energy of supercells of increasing size (each formed from the same H-isomer), and we apply to all system sizes (including the thermodynamic limit) the EAC that is computed for the smallest system; that is, we assume the EAC is independent of N.

We can gauge the error introduced by this approximation by computing the EAC for a $2 \times 2 \times 2$ ($n_c = 2$) supercell. The result is included in Figure 2 as the green line labeled "$2 \times 2 \times 2$ supercell." This difference should be compared to the EAC for the $1 \times 1 \times 1$ ($n_c = 1$) supercell, given in the figure by the blue solid line labeled "$U_{0,i} + A_{\mathrm{harm},i}$." The comparison shows that for T above about 150 K, the EACs differ by about ~10% of the EAC itself. The EAC is in turn only 25% as large as the finite-size effect in going from the $n_c = 1$ to the $n_c = 2$ supercell (described below). Another factor to consider is the use of a finite number of samples (100) in computing the exponential averages. This leads to an uncertainty of about 5% in the $n_c = 1$ EAC (blue curve) ~0.007 (and 0.003 kJ/mol for $T = 100$ and 300 K, respectively), which may account for some of the difference with the $n_c = 2$ EAC. In sum, the results suggest that for $T > 150$ K, it is reasonable to use the $n_c = 1$ EAC as a surrogate for the corresponding correction at each system size, including the thermodynamic limit.

The summation over $\ln \omega_i$ in eq 4 is the only nontrivial N-dependent term of the classical harmonic free energy. According to Hoover,[69] the leading N dependence of this summation should be $\ln N/N$, so in subtracting this contribution from the sum in eq 4 we should produce a system-size dependence that is closer to linear in $1/N$. Hoover's conclusion was based on observations of the analytic behavior for a 1D harmonic system, and numerical results for systems in 2D and 3D, both involving only translational degrees of freedom. Figure 3 confirms that his analysis is correct also for molecular systems, in that the data are clearly more linear in $1/N$ when $\ln N/N$ is subtracted ($C = 1$). This suggests that the general trend observed by Hoover, viz., that the $\ln N/N$ leading term of the free energy is independent of the number of dof per molecule, persists even with rotational motions included. In addition, although the extrapolation to infinite system size ($1/N \rightarrow 0$) yields a different intercept for each structure, the slopes are nearly equal (differing by from each other by less than 0.5%).

For the quantum system, unlike the classical treatment, the extrapolation to infinite system size depends on the temperature (see eq 5). Moreover, since the quantum and classical behavior are the same only for high temperatures, we can count on $\ln N/N$ to be the leading term only under those conditions. We performed fits of the harmonic free energy with the $\ln N/N$

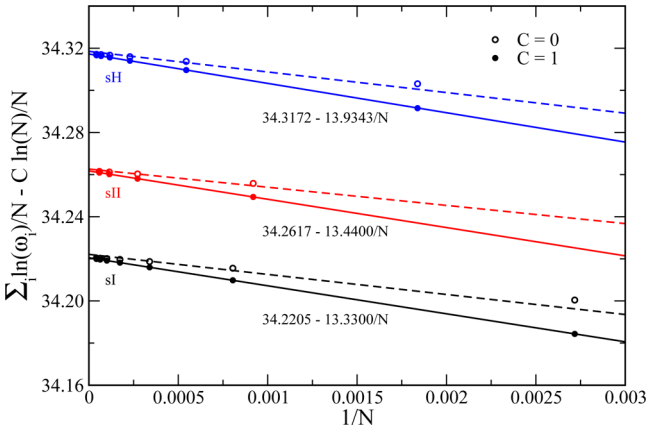

Figure 3. Finite-size effects on the classical harmonic free energy for the sI, sII, and sH structures. The filled points are harmonic free-energy contributions with the leading $\ln N/N$ term subtracted ($C = 1$), and the open circles are the raw data ($C = 0$). Dashed and solid lines are linear fits (in $1/N$) to the $C = 0$ and $C = 1$ cases, respectively. Note that the results for the smallest N for each structure are not shown, as they are off the scale to the right; however all points are included in the linear fits.

contribution removed (as with the classical case), regressing a new curve for each temperature. We find that the linear fit is inadequate at lower temperatures, but that a quadratic form (in $1/N$) was effective in describing the data. The fit matches the data to within 10^{-6} kJ/mol, which is on the same order as the convergence tolerance in the lattice and Ewald sums. We do not show plots of the fits and instead just present the $N \rightarrow \infty$ values in the next section.

3.4. Free-Energy Results. Figures 4 (classical) and 5 (quantum) show the harmonic Helmholtz free energies

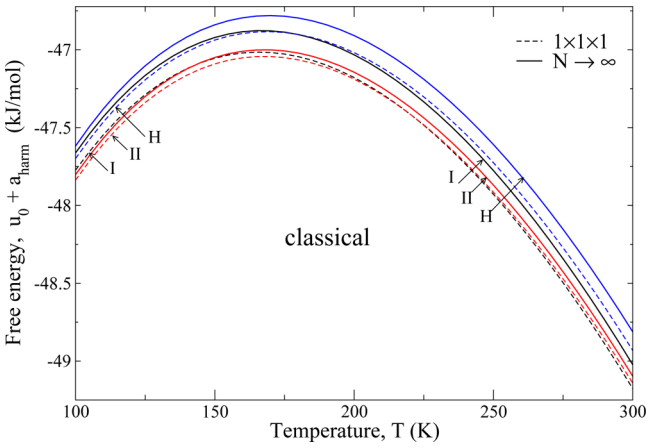

Figure 4. Classical harmonic Helmholtz free energy, per unit molecule, for the sI, sII, and sH structures as a function of temperature in the thermodynamic limit (solid lines) and for a single unit cell (dashed lines). The exponential-averaging correction is included in all curves.

(including the EAC correction) in the thermodynamic limit versus temperature. In the whole temperature range (100 to 300 K), sII has the lowest free energy according to both treatments; however, it is almost indistinguishable from sI according to the quantum treatment while, classically, the difference is noticeable. The systems are not all at the same density (differing from each other by about 1%), so we cannot draw conclusions about relative stability from these data, and

dx.doi.org/10.1021/ie504008h | Ind. Eng. Chem. Res. 2015, 54, 4487−4496

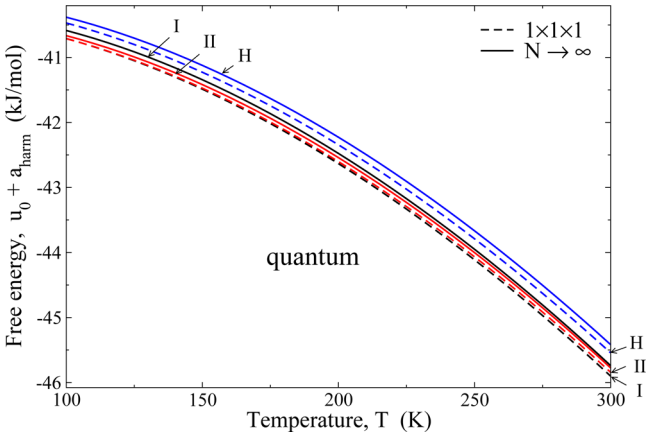

Figure 5. Quantum harmonic Helmholtz free energy, per unit molecule, for the sI, sII, and sH structures as a function of temperature in the thermodynamic limit (solid lines) and for a single unit cell (dashed lines). The exponential-averaging correction is included in all curves.

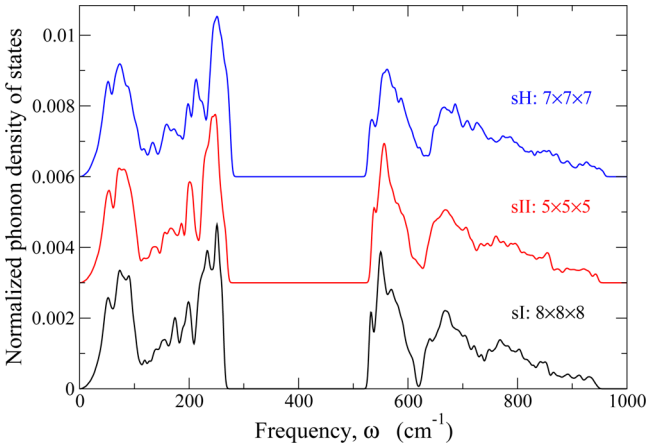

Figure 6. Normalized phonon density-of-states (PDOS) of the largest supercells considered in this work for sI, sII, and sH structures. sI and sII are shifted in *y*-axis by 0.006 and 0.003, respectively, from sH to avoid overlap.

such conclusions are not the goals of this study. Regardless, it is known that the empty lattices are all unstable relative to ice phases.[70,71]

The nearly equal slopes of the harmonic free energy with $1/N$ (cf. Figure 3) suggest that finite-size effects impact all crystal structures nearly equally, so if the interest is only in computing differences between the structures, then a small system would suffice. However, in many studies the comparison is made for convenience between systems of the same number of unit cells N_c, not the same number of molecules N. To demonstrate the effect of comparing free energies in this manner, Figures 4 and 5 show free energy curves based on calculation for a single unit cell. In both the quantum and classical treatments, differences in free energy between structures decrease markedly when using only one unit cell, and the effect is strong enough to affect the ordering of the curves. For the quantum treatment, the free energies of the sI and sII structures when each are described by a single unit cell are indistinguishable around 100 K before they become different for high temperature; for the infinite system, their relative behavior is in fact the opposite of this trend.

Our single unit cell results show a qualitative agreement with that of Tanaka et al.[70,71] for empty sI and sII structures. We do not expect an exact agreement, for several reasons: they averaged (in an unspecified manner) their results over only six proton-disordered structures; we used a different technique to calculate the long-range Coulomb interactions and employed much larger cutoffs for the dispersion interactions; also, they did not include the s_{rot} contribution (eqs 4 and 5).

3.5. Phonon Density of States. Figure 6 shows the phonon density-of-states (PDOS) for the largest system sizes studied in this work. The high-resolution, high-precision histogram was built using at least 100 000 normal modes for each of the three empty clathrate structures, with narrow-width (σ = 4 cm^{-1}) Gaussian smearing used to smooth the data. One common feature of all structures is the existence of a large gap separating two different bands. Based on eigenvector arguments, the lower and upper bands are mostly for translation and rotation modes, respectively.[22,23,37] Our PDOS results show good agreement with previous work.[22,23,35,37,71−73]

3.6. Accuracy of the Local-Harmonic Approximation. Although results for the local-harmonic approximation (LHA) were reported previously for different clathrate hydrates,[50−52] comparison with the full harmonic free energy was not performed. Figure 7 shows such a comparison for our three

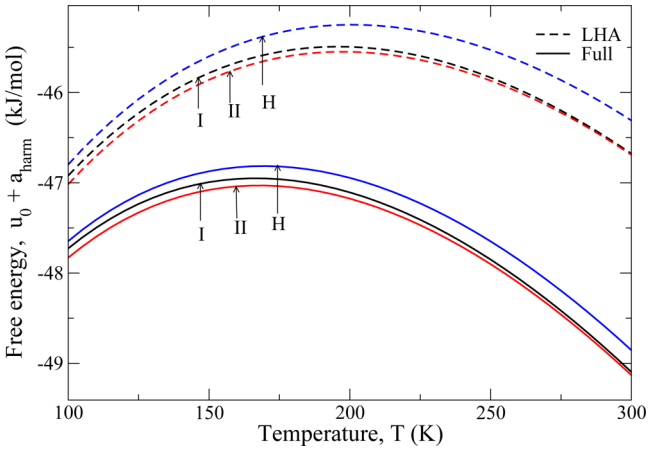

Figure 7. Relative stability based on classical free energies of single H-isomer (the minimum), in the thermodynamic limit, of sI, sII, and sH structures using full and local harmonic (LHA) methods.

structures in the thermodynamic limit. In this temperature range, the absolute free energies differ by at least 0.8 kJ/mol. Although this difference increases with the temperature, the relative ordering of the structures is preserved.

4. CONCLUSIONS

The analysis performed here aims to demonstrate the significance of finite-size effects and proton disorder when performing lattice dynamics calculations to estimate the free energy of clathrate structures. Although the development involves the evaluation and comparison of free energies for different structures, we do not mean for these results to be interpreted in regard to the relative stability of the structures, nor to identify a phase transition. We do not, for example, include guest molecules at all, and we do not attempt to ensure that the systems are at a common pressure or even at the same density. Instead, the comparisons are made to provide a sense of the variation of the free energy between structures, so as to provide a scale for gauging the magnitude of the effects under study.

dx.doi.org/10.1021/ie504008h | Ind. Eng. Chem. Res. 2015, 54, 4487−4496

Within this context, the results demonstrate that the effects involved can be significant. We can summarize some of the key considerations (some of which are already known and thus were not detailed above), keeping in mind that the scale of the difference in free energies between the empty structures is at most 0.2 kJ/mol.

Finite size effects (one unit cell versus the infinite system) are, at 300 K, in the range of 0.15 to 0.5 kJ/mol, depending on crystal structure. Of particular importance is the need to compare systems having equal (or nearly equal) numbers of molecules, rather than comparing systems having the same number of unit cells (which often is only a single cell). The error in the free-energy difference between structures incurred by using a single unit cell can be on the order of 0.4 kJ/mol.

Proton disorder (as measured by the exponential-averaging correction) affects the free energy by about 0.03 to 0.06 kJ/mol, again depending on crystal structure.

Quantum effects are on the order of 5 kJ/mol and differ between structures by about 0.1 kJ/mol.

Point defects, including vacancies, interstitials, and Bjerrum defects are stable at equilibrium and can affect the free energy. We do not have data regarding defects in clathrates, but calculations have been performed for ice structures (e.g., ref 74).

We also wish to point out the usefulness of the well-established methodology for analytic evaluation of orientational derivatives of rigid molecules, which can be used to avoid numerical differentiation; the relevant equations are summarized in the Supporting Information. We mention this because, while some researchers do perform derivative evaluations in the same manner that we have, it is also not unusual to encounter studies that use numerical evaluation of derivatives. Such an approach can be computationally expensive when also doing Ewald and lattice sums. In this regard, our formulation for the elements of the dynamical matrix, eq 8, is particularly efficient when studying systems requiring Ewald summation. Also of note is the observation that the leading-order finite-size correction for classical molecular systems is $-\ln N/N$, as is known for monatomic molecules.

It would be of interest to extend these studies to put them in the context of occupied clathrate systems. It would also be worthwhile to conduct a similar study for the various phases of ice. With the development of very efficient methods for evaluation of anharmonic contributions to the free energy,[46,47] we may soon find that proton disorder and finite-size effects will prove to be the limiting factor in obtaining accurate free energies. These effects can be efficiently handled with lattice-dynamics methods, which ultimately will be used as a key part of an analytical + simulation strategy for the calculation of solid-state phase diagrams from first principles.

■ ASSOCIATED CONTENT

Supporting Information

Detailed equations needed to obtain the molecular force constants in terms of the "normal" atomic force constants are provided. Using the TIP4P model, with Ewald sum for the Coulomb interactions, the atom−atom force constant formulas are given. This material is available free of charge via the Internet at http://pubs.acs.org/.

■ AUTHOR INFORMATION

Corresponding Author

*E-mail: kofke@buffalo.edu.

Notes

The authors declare no competing financial interest.

■ ACKNOWLEDGMENTS

Acknowledgment is made to the Donors of the American Chemical Society Petroleum Research Fund for partial support of this research. Funding was also provided by an IMPACT grant from the University at Buffalo.

■ REFERENCES

(1) Sloan, E.; Koh, C. *Clathrate Hydrates of Natural Gases*, 3rd ed.; Chemical Industries, Taylor & Francis, 2007.

(2) Koh, C. A.; Sloan, E. D.; Sum, A. K.; Wu, D. T. Fundamentals and Applications of Gas Hydrates. *Annu. Rev. Chem. Biomol. Eng.* **2011**, *2*, 237−257.

(3) Lee, H.; Lee, J. W.; Kim, D. Y.; Park, J.; Seo, Y. T.; Zeng, H.; Moudrakovski, I. L.; Ratcliffe, C. I.; Ripmeester, J. A. Tuning clathrate hydrates for hydrogen storage. *Nature* **2005**, *434*, 743−746.

(4) Struzhkin, V. V.; Militzer, B.; Mao, W. L.; Mao, H. k.; Hemley, R. J. Hydrogen Storage in Molecular Clathrates. *Chem. Rev.* **2007**, *107*, 4133−4151.

(5) Strobel, T. A.; Hester, K. C.; Koh, C. A.; Sum, A. K.; Sloan, E. D. Properties of the clathrates of hydrogen and developments in their applicability for hydrogen storage. *Chem. Phys. Lett.* **2009**, *478*, 97−109.

(6) Rochelle, C. A.; Camps, A. P.; Long, D.; Milodowski, A.; Bateman, K.; Gunn, D.; Jackson, P.; Lovell, M. A.; Rees, J. *Can CO_2 hydrate assist in the underground storage of carbon dioxide?*; Geological Society: London; Special Publications 2009, Vol *319*, pp 171−183.

(7) Boswell, R. Is Gas Hydrate Energy Within Reach? *Science* **2009**, *325*, 957−958.

(8) Kang, S. P.; Lee, H. Recovery of CO_2 from Flue Gas Using Gas Hydrate: Thermodynamic Verification through Phase Equilibrium Measurements. *Environ. Sci. Technol.* **2000**, *34*, 4397−4400.

(9) Bradshaw, R. W.; Greathouse, J. A.; Cygan, R. T.; Simmons, B. A.; Dedrick, D. E.; Majzoub, E. H. *Desalination Utilizing Clathrate Hydrates*; LDRD Final Report SAND2007-6565, 2008.

(10) Fournaison, L.; Delahaye, A.; Chatti, I.; Petitet, J. P. CO_2 Hydrates in Refrigeration Processes. *Ind. Eng. Chem. Res.* **2004**, *43*, 6521−6526.

(11) Ogawa, T.; Ito, T.; Watanabe, K.; Tahara, K.; Hiraoka, R.; Ochiai, J.; Ohmura, R.; Mori, Y. H. Development of a novel hydrate-based refrigeration system: A preliminary overview. *Appl. Therm. Eng.* **2006**, *26*, 2157−2167.

(12) Sum, A. K.; Wu, D. T.; Yasuoka, K. Energy science of clathrate hydrates: Simulation-based advances. *MRS Bull.* **2011**, *36*, 205−210.

(13) McMullan, R. K.; Jeffrey, G. A. Polyhedral Clathrate Hydrates. IX. Structure of Ethylene Oxide Hydrate. *J. Chem. Phys.* **1965**, *42*, 2725−2732.

(14) Mak, T. C. W.; McMullan, R. K. Polyhedral Clathrate Hydrates. X. Structure of the Double Hydrate of Tetrahydrofuran and Hydrogen Sulfide. *J. Chem. Phys.* **1965**, *42*, 2732−2737.

(15) Ripmeester, J. A.; John, S. T.; Ratcliffe, C. I.; Powell, B. M. A new clathrate hydrate structure. *Nature* **1987**, *325*, 135−136.

(16) van der Waals, J. H. The statistical mechanics of clathrate compounds. *Trans. Faraday Soc.* **1956**, *52*, 184−193.

(17) Platteeuw, J. C.; van der Waals, J. H. Thermodynamic properties of gas hydrates II: Phase equilibria in the system H_2S-C_3H_3-H_2O at −3°C. *Recl. Trav. Chim. Pays-Bas* **1959**, *78*, 126−133.

(18) Wierzchowski, S. J.; Monson, P. A. Calculation of Free Energies and Chemical Potentials for Gas Hydrates Using Monte Carlo Simulations. *J. Phys. Chem. B* **2007**, *111*, 7274−7282.

(19) Pimpalgaonkar, H.; Veesam, S. K.; Punnathanam, S. N. Theory of Gas Hydrates: Effect of the Approximation of Rigid Water Lattice. *J. Phys. Chem. B* **2011**, *115*, 10018−10026.

(20) Ravipati, S.; Punnathanam, S. N. Analysis of Parameter Values in the van der Waals and Platteeuw Theory for Methane Hydrates Using

Monte Carlo Molecular Simulations. *Ind. Eng. Chem. Res.* **2012**, *51*, 9419−9426.
(21) van Klaveren, E. P.; Michels, J. P. J.; Schouten, J. A.; Klug, D. D.; Tse, J. S. Stability of doubly occupied N_2 clathrate hydrates investigated by molecular dynamics simulations. *J. Chem. Phys.* **2001**, *114*, 5745−5754.
(22) Inerbaev, T.; Belosludov, V.; Belosludov, R.; Sluiter, M.; Kawazoe, Y.; Kudoh, J. Theoretical study of clathrate hydrates with multiple occupation. *J. Inclusion Phenom. Mol. Recognit. Chem.* **2004**, *48*, 55−60.
(23) Inerbaev, T.; Belosludov, V.; Belosludov, R.; Sluiter, M.; Kawazoe, Y. Dynamics and equation of state of hydrogen clathrate hydrate as a function of cage occupation. *Comput. Mater. Sci.* **2006**, *36*, 229−233.
(24) Belosludov, V. R.; Subbotin, O. S.; Krupskii, D. S.; Belosludov, R. V.; Kawazoe, Y.; Kudoh, J. Physical and chemical properties of gas hydrates: Theoretical aspects of energy storage application. *Mater. Trans.* **2007**, *48*, 704−710.
(25) Alavi, S.; Woo, T. K. How much carbon dioxide can be stored in the structure H clathrate hydrates?: A molecular dynamics study. *J. Chem. Phys.* **2007**, *126*, 044703.
(26) Katsumasa, K.; Koga, K.; Tanaka, H. On the thermodynamic stability of hydrogen clathrate hydrates. *J. Chem. Phys.* **2007**, *127*, 044509.
(27) Knott, B. C.; Molinero, V.; Doherty, M. F.; Peters, B. Homogeneous Nucleation of Methane Hydrates: Unrealistic under Realistic Conditions. *J. Am. Chem. Soc.* **2012**, *134*, 19544−19547.
(28) Wierzchowski, S. J.; Monson, P. A. Studies of a primitive model of mixtures of nonpolar molecules with water. *Mol. Phys.* **2004**, *102*, 2071−2079.
(29) Wierzchowski, S. J.; Monson, P. A. Calculating the Phase Behavior of Gas-Hydrate-Forming Systems from Molecular Models. *Ind. Eng. Chem. Res.* **2006**, *45*, 424−431.
(30) Nakayama, T.; Koga, K.; Tanaka, H. Augmented stability of hydrogen clathrate hydrates by weakly polar molecules. *J. Chem. Phys.* **2009**, *131*, 214506.
(31) Conde, M. M.; Vega, C.; Tribello, G. A.; Slater, B. The phase diagram of water at negative pressures: Virtual ices. *J. Chem. Phys.* **2009**, *131*, 034510.
(32) Conde, M. M.; Vega, C. Determining the three-phase coexistence line in methane hydrates using computer simulations. *J. Chem. Phys.* **2010**, *133*, 064507.
(33) Jensen, L.; Thomsen, K.; von Solms, N.; Wierzchowski, S.; Walsh, M. R.; Koh, C. A.; Sloan, E. D.; Wu, D. T.; Sum, A. K. Calculation of Liquid Water-Hydrate-Methane Vapor Phase Equilibria from Molecular Simulations. *J. Phys. Chem. B* **2010**, *114*, 5775−5782.
(34) Kolafa, J. Residual entropy of ices and clathrates from Monte Carlo simulation. *J. Chem. Phys.* **2014**, *140*, 204507.
(35) Tanaka, H.; Kiyohara, K. On the thermodynamic stability of clathrate hydrate. I. *J. Chem. Phys.* **1993**, *98*, 4098−4109.
(36) Tanaka, H.; Kiyohara, K. The thermodynamic stability of clathrate hydrate. II. Simultaneous occupation of larger and smaller cages. *J. Chem. Phys.* **1993**, *98*, 8110−8118.
(37) Belosludov, V.; Lavrentiev, M.; Dyadin. Dynamic and thermodynamic properties of clathrate hydrates. *J. Inclusion Phenom. Mol. Recognit. Chem.* **1990**, *8*, 59−69.
(38) Tanaka, H. Thermodynamic stability and negative thermal expansion of hexagonal and cubic ices. *J. Chem. Phys.* **1998**, *108*, 4887−4893.
(39) Belosludov, V. R.; Inerbaev, T. M.; Subbotin, O. S.; Belosludov, R. V.; Kudoh, J.; Kawazoe, Y. Thermal expansion and lattice distortion of clathrate hydrates of cubic structures I and II. *J. Supramol. Chem.* **2002**, *2*, 453−458.
(40) Umemoto, K.; Wentzcovitch, R. M.; de Gironcoli, S.; Baroni, S. Order−disorder phase boundary between ice VII and VIII obtained by first principles. *Chem. Phys. Lett.* **2010**, *499*, 236−240.
(41) Ramrez, R.; Neuerburg, N.; Fernández-Serra, M.-V.; Herrero, C. P. Quasi-harmonic approximation of thermodynamic properties of ice Ih, II, and III. *J. Chem. Phys.* **2012**, *137*, 044502.
(42) Ramirez, R.; Neuerburg, N.; Herrero, C. P. The phase diagram of ice Ih, II, and III: A quasi-harmonic study. *J. Chem. Phys.* **2012**, *137*, 134503.
(43) Ramírez, R.; Neuerburg, N.; Herrero, C. P. The phase diagram of ice: A quasi-harmonic study based on a flexible water model. *J. Chem. Phys.* **2013**, *139*, 084503.
(44) Monson, P. A.; Kofke, D. A. Solid-Fluid Equilibrium: Insights from Simple Molecular Models. *Adv. Chem. Phys.* **2000**, *115*, 113−179.
(45) Tan, T. B.; Schultz, A. J.; Kofke, D. A. Suitability of umbrella- and overlap-sampling methods for calculation of solid-phase free energies by molecular simulation. *J. Chem. Phys.* **2010**, *132*, 214103.
(46) Tan, T. B.; Schultz, A. J.; Kofke, D. A. Efficient calculation of temperature dependence of solid-phase free energies by overlap sampling coupled with harmonically targeted perturbation. *J. Chem. Phys.* **2010**, *133*, 134104.
(47) Tan, T. B.; Schultz, A. J.; Kofke, D. A. Efficient calculation of α- and β-nitrogen free energies and coexistence conditions via overlap sampling with targeted perturbation. *J. Chem. Phys.* **2011**, *135*, 044125.
(48) Moustafa, S. G.; Schultz, A. J.; Kofke, D. A. A comparative study of methods to compute the free energy of an ordered assembly by molecular simulation. *J. Chem. Phys.* **2013**, *139*, 084105.
(49) Takeuchi, F.; Hiratsuka, M.; Ohmura, R.; Alavi, S.; Sum, A. K.; Yasuoka, K. Water proton configurations in structures I, II, and H clathrate hydrate unit cells. *J. Chem. Phys.* **2013**, *138*, 124504.
(50) Westacott, R.; Rodger, P. Full-coordinate free-energy minimisation for complex molecular crystals:Type I hydrates. *Chem. Phys. Lett.* **1996**, *262*, 47−51.
(51) Westacott, R.; Rodger, P. Direct free energy calculations for gas hydrate. *Abstr. Pap. Am. Chem. Soc.* **1997**, *213*, 539−543.
(52) Westacott, R. E.; Rodger, P. M. A local harmonic study of clusters of water and methane. *J. Chem. Soc., Faraday Trans.* **1998**, *94*, 3421−3426.
(53) Born, M.; Huang, K. *Dynamical Theory of Crystal Lattices*; International Series of Monographs on Physics, Clarendon Press, 1954.
(54) Dove, M. T. *Introduction to Lattice Dynamics*; Cambridge University Press: New York, 2005.
(55) Venkataraman, G.; Sahni, V. C. External vibrations in complex crystals. *Rev. Mod. Phys.* **1970**, *42*, 409−470.
(56) Belosludov, R.; Igumenov, I.; Belosludov, V.; Shpakov, V. Dynamical and thermodynamical properties of the acetylacetones of copper, aluminium, indium, and rhodium. *Mol. Phys.* **1994**, *82*, 51−66.
(57) McQuarrie, D. A. *Statistical Mechanics*; Harper's Chemistry Series; Harper Collins Publishing, Inc.: New York, 1976.
(58) Moustafa, S. G.; Schultz, A. J.; Kofke, D. A. Efficient harmonic free energy calculations of nonlinear rigid molecular crystals: I. Theory. *J. Chem. Phys.* To be published.
(59) Maradudin, A. A.; Montroll, E. W.; Weiss, G. H.; Ipatova, I. P. *Theory of Lattice Dynamics in the Harmonic Approximation*, 2nd ed.; Solid State Physics, Academic Press: New York, 1971; Vol. Supplement 3.
(60) Bernal, J. D.; Fowler, R. H. A Theory of Water and Ionic Solution, with Particular Reference to Hydrogen and Hydroxyl Ions. *J. Chem. Phys.* **1933**, *1*, 515−548.
(61) Singer, S. J.; Knight, C. Hydrogen-Bond Topology and Proton Ordering in Ice and Water Clusters. *Adv. Chem. Phys.* **2012**, *147*, 1−74.
(62) Bjerrum, N. Structure and Properties of Ice. *Science* **1952**, *115*, 385−390.
(63) Pauling, L. The Structure and Entropy of Ice and of Other Crystals with Some Randomness of Atomic Arrangement. *J. Chem. Phys.* **1935**, *57*, 2680−2684.
(64) Buch, V.; Sandler, P.; Sadlej, J. Simulations of H_2O Solid, Liquid, and Clusters, with an Emphasis on Ferroelectric Ordering Transition in Hexagonal Ice. *J. Phys. Chem. B* **1998**, *102*, 8641−8653.
(65) Jorgensen, W. L.; Chandrasekhar, J.; Madura, J. D.; Impey, R. W.; Klein, M. L. Comparison of simple potential functions for simulating liquid water. *J. Chem. Phys.* **1983**, *79*, 926−935.
(66) Ewald, P. P. Die Berechnung optischer und elektrostatischer Gitterpotentiale. *Ann. Phys. (Berlin, Ger.)* **1921**, *369*, 253−287.

(67) Kolafa, J.; Perram, J. W. Cutoff errors in the Ewald summation formulae for point charge systems. *Mol. Simul.* **1992**, *9*, 351−368.
(68) LeSar, R.; Najafabadi, R.; Srolovitz, D. J. Finite-temperature defect properties from free-energy minimization. *Phys. Rev. Lett.* **1989**, *63*, 624−627.
(69) Hoover, W. G. Entropy for Small Classical Crystals. *J. Chem. Phys.* **1968**, *49*, 1981−1982.
(70) Tanaka, H.; Nakanishi, K. The Stability of Clathrate Hydrates: Temperature Dependence of Dissociation Pressure in Xe and Ar Hydrate. *Mol. Simul.* **1994**, *12*, 317−327.
(71) Tanaka, H. A novel approach to the stability of clathrate hydrate. *Fluid Phase Equilib.* **1995**, *104*, 331−340.
(72) Tanaka, H.; Tamai, Y.; Koga, K. Large Thermal Expansivity of Clathrate Hydrates. *J. Phys. Chem. B* **1997**, *101*, 6560−6565.
(73) Tanaka, H.; Matsumoto, M. On the Thermodynamic Stability of Clathrate Hydrates V: Phase Behaviors Accommodating Large Guest Molecules with New Reference States. *J. Phys. Chem. B* **2011**, *115*, 14256−14262.
(74) de Koning, M.; Antonelli, A. Modeling equilibrium concentrations of Bjerrum and molecular point defects and their complexes in ice I_h. *J. Chem. Phys.* **2008**, *128*, 164502.